Rifts in Spreading Wax Layers

Rolf Ragnarsson, J. Lewis Ford,* Christian D. Santangelo, and Eberhard Bodenschatz†
Laboratory of Atomic and Solid State Physics, Cornell University, Ithaca, New York 14853-2501
(Received 20 October 1995)

We report results on the rift formation between two freezing wax plates floating on molten wax which are pulled apart with constant velocity. Several distinct patterns were observed for increasing spreading rates; a stable straight rift, a spiky rift with fracture zones almost parallel to the spreading direction, and a regular zigzag pattern characterized by an angle dependent on the spreading rate. The characteristic angles of the zigzag pattern agree with a simple geometrical model. The coarsening of the pattern over time and the three-dimensional structure of the crust are also discussed. [S0031-9007(96)00113-5]

PACS numbers: 91.45.–c, 44.90.+c, 64.60.Cn, 91.60.Ba

Pattern formation due to morphological instabilities has recently attracted considerable interest [1]. Prominent examples are in directional solidification [2] and fracture patterns [3]. Here we present results on a pattern forming system where solidification, fracture, and creep are important.

Our investigations were motivated by experiments that were conducted earlier in an attempt to model the development of transform faults of the Earth's crust as observed between two separating tectonic plates [4–6]. In these experiments molten wax was frozen at the surface by a flow of cold air. Then the solid crust was pulled apart with constant velocity and a rift was formed separating the crust into two solid plates. A straight rift, initially perpendicular to the pulling direction, was found to evolve into a pattern consisting of straight segments interrupted by faults parallel to the pulling direction. The pattern was interpreted to resemble the transform faults of the midocean ridges and a model based on shrinkage and the mechanical properties of the wax was proposed [5]. At slower spreading rates a rift consisting of oblique segments was also observed [5,6]. However, no further investigation of this latter phenomenon was undertaken and to date any detailed knowledge of the phase diagram is lacking.

In this Letter we report on the systematic experimental investigation of the rift formation of the paraffin wax system as a function of spreading velocity. We found several distinct spreading regimes, each characterized by a unique type of rift pattern. At low spreading velocities we discovered a novel, "spiky" rift pattern dominated by fracture zones. At higher pulling speeds we found a transition to a regular "zigzag" pattern, which with increasing pulling speed became steeper and steeper, finally forming a pattern of faultlike slips parallel to the spreading direction separated by straight regions perpendicular to it. We show that in the zigzag regime the angle of the oblique rift segments can be described by a simple geometrical model, suggesting a pattern formation mechanism also found in other front propagation problems [7].

Motivated by the prior experimental investigations [5], we used Shellwax 120, a macrocrystalline paraffin wax [8]. Shellwax 120 crystallizes at 54 °C and has a solid-solid phase transition at about 35 °C [9]. While the first solid phase is plastic and easily deformable, the second is hard and brittle. Upon freezing, the wax shrinks in the temperature range from 54 to 46 °C by roughly 10% and by another 4% from 35 to 28 °C [9].

The experimental setup, as shown schematically in Fig. 1, consists of a rectangular tray of dimensions $114 \times 36 \times 10$ cm^3 with stainless steel side walls and an aluminum bottom. It was filled to a height of 8 cm with Shellwax 120. The bottom was heated by a regulated circulating water bath to 57.5 ± 0.05 °C, slightly above the 54 °C melting temperature of Shellwax 120. To solidify the wax surface, air of temperature 25.5 ± 0.5 °C was blown across the long side of the apparatus. No effect of this introduced anisotropy on the pattern

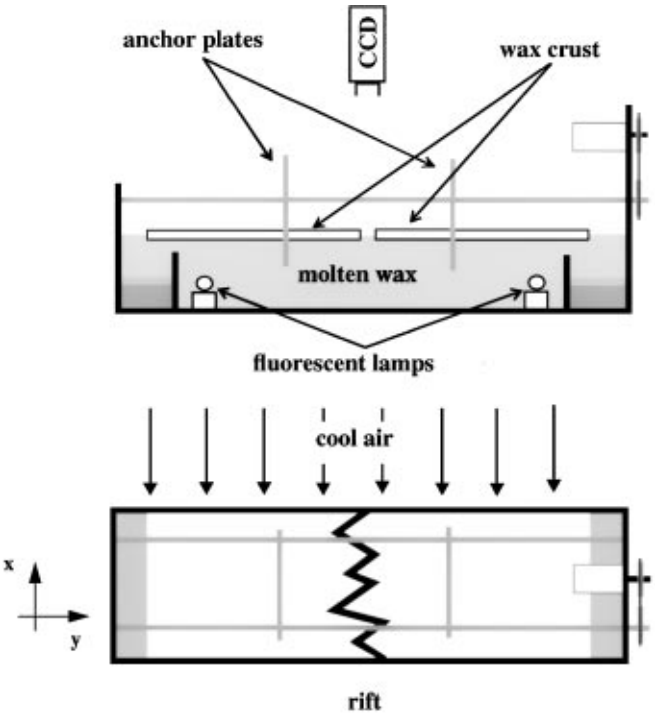

FIG. 1. Experimental setup schematically: side and top.

 0031-9007/96/76(18)/3456(4)$10.00

formation was observed. Two vertical stainless steel anchor plates of 3 mm thickness were frozen into the wax. A microstepping motor was used to move the two anchor plates apart, each at the same speed, ranging from 1 μm/sec to 1 mm/sec. To avoid a buildup of solid wax at the ends of the tray, each wax crust was melted off in warmer regions of lateral size 10×20 cm^2. Each region was heated by an electric film heater mounted on an aluminum plate of size $100 \times 200 \times 3$ mm^3 and insulated from the temperature controlled bottom by a layer of 3 cm thick polyurethane foam. To minimize thermal cross talk, two 6 cm high stainless steel plates separated the warmer regions from the main part of the tray, allowing the solid crust to pass over. The wax layer was illuminated from below by two fluorescent lamps placed into the molten wax and extending over the width of the tray, allowing the rift to be visualized from above with a charge coupled device (CCD) camera connected to a digital image processing system. Because of light diffusing properties of the rigid wax, the crust appeared white, while closer to the rift the ductile wax was darker, and regions of molten wax appeared black.

In a typical run, first the cooling air was turned off and all the wax was melted. The anchor plates were positioned about 5 cm apart and the cooling air was turned on again. After about 10 min the wax had solidified to a rigid crust approximately 2 mm thick as measured from a cutout of the solidifying wax. The equilibrium wax thickness was measured by a cutout to be roughly 1 cm. To ensure better reproducibility a straight rift was cut with a sharp knife parallel to the anchor plates. No change of the late stage pattern formation behavior was observed when the wax layer was torn instead of being cut. At $t = 0$ the microstepping motor was turned on and moved the two wax plates apart with constant velocity. The newly created crust had a thickness less than 2 mm again measured from a cutout. During the run digital images of the rift were taken at constant time intervals. A run ended when the anchor plates reached the warmer regions.

Rift patterns obtained at four different spreading rates are shown in Fig. 2. The images were taken after a time t when initial transients had died out and clearly illustrate the existence of different rift formation regimes.

For plate pulling speeds (or, equivalently, spreading rates) $v \leq 40$ μm/sec, a straight rift remained flat and frozen over as shown in Fig. 2(a). For $40 < v \leq 120$ μm/sec, a spiky rift pattern developed. The rift was dominated by oblique rift segments [Fig. 2(b)], which for increased spreading rate were almost parallel to the spreading direction. The oblique rift segments were frozen over and showed fracture and rift slippage. These regions were hardly visible in a linearly scaled gray scale image and a false color map was used in Fig. 3(a) to enhance the rift structure. Thick frozen wax corresponds to blue, thinner frozen wax is green or yellow, and upwelling hot liquid wax is red. It is remarkable that the rift is torn only in a few places where the rift segments are almost perpendicular to the spreading direction.

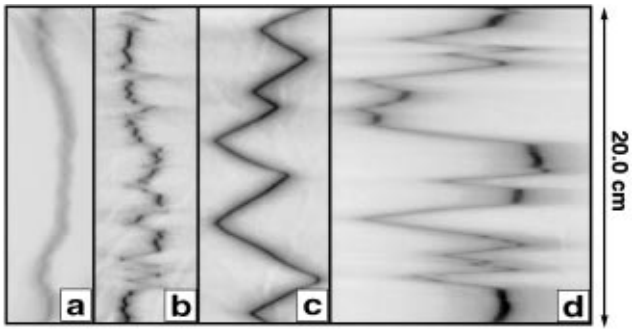

FIG. 2. Rift patterns at different spreading rates (a) $v = 35$ μm/sec, $t = 4800$ sec; (b) $v = 85$ μm/sec, $t = 1900$ sec; (c) $v = 177$ μm/sec, $t = 1400$ sec; (d) $v = 709$ μm/sec, $t = 360$ sec.

In the range of $120 < v \leq 170$ μm/sec, the spiky pattern coexisted with a regular zigzag pattern [Fig. 3(b)], which was the selected rift structure for $v > 170$ μm/sec, as shown in Figs. 2(c) and 4. In the zigzag region we did not observe the partial freezing of the rift that characterized the spiky state. Instead, the rift was open along its whole length, as evidenced by the uniformly black color of the rift in Figs. 2(c) and 4. Two solidification fronts propagating from each crust solidified the upwelling wax. Contrary to the spiky regime, where

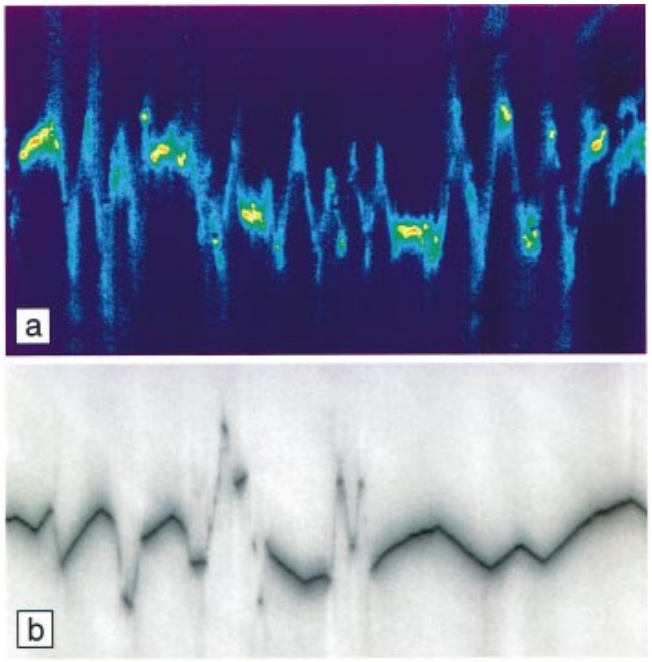

FIG. 3 (color). (a) Rift structure in false color for ($v = 107$ μm/sec, $t = 2400$ sec). Torn regions of molten upwelling wax are red, while crystallized wax is blue. (b) Rift structure in the coexistence region ($v = 142$ μm/sec, $t = 2250$ sec). The width of the image corresponds to 20 cm.

stress and temperature field must be important factors for the rift formation, here the two fronts can interact only via the temperature field. Upwelling hot wax, latent heat release due to solidification at each edge of the rift [10], and cooling air temperature are the obvious factors determining the width of the rift.

With increasing spreading rate the oblique rift segments became steeper and steeper, finally forming a pattern of faultlike slips parallel to spreading direction separated by straight regions perpendicular to it [Fig. 2(d)].

The solid crust behind the rift had a topography of crests and valleys as shown in Fig. 4. To visualize the crustal topography, the fluorescent lamps were angled slightly off the x axis adding illumination from the side. Regions tilted towards the high intensity side scatter more light and appear brighter than regions tilted away from the high intensity side of the tray. The crustal topography may be explained by the fact that the crust along any line parallel to the x axis varied in age; i.e., the crust further from the rift was created earlier and had cooled for a longer time, leading to an increased thickness. While cooling, the older crust shrunk and stresses developed pulling the younger regions apart. As a result a straight line of ductile wax (crest) was left behind the pointed side of the apices. The crests were elevated by about 1 mm relative to the bottom of valleys built by the oldest wax. This topography can be understood by the shrinkage of the crystalline wax at the surface while the wax below was still in its ductile phase.

In order to systematically characterize the rift patterns, we measured the local angle between the rift and the x axis (see Fig. 1). From the digital images the position of the rift (x_i, y_i) was found by locating the darkest pixel along each row parallel to the y axis. The obtained set of points $y_i(x_i)$ was smoothed three times with a three-point running average in order to minimize effects due to finite CCD pixel resolution. We then calculated the slope with a fourth-order finite difference formula and from it the characteristic angle $\varphi_i(x_i)$. The angles φ_i were plotted in a histogram, where each bin count was weighted by the length of each segment. The maximum of the histogram was chosen to be the characteristic rift angle φ. Figure 5 shows the characteristic angles obtained for different pulling speeds. The plot shows the selected angles of both the spiky regime at slow spreading rates and the zigzag regime at faster spreading rates. While the angle in the spiky regime rapidly approaches the limit of 90° causing fracture and rift slippage, the angle in the zigzag regime increases more gradually.

In the zigzag regime we observed that the rift width was approximately constant up to spreading rates of about 500 μm/sec. Given constant temperature at the wax-air interface, for a rift with constant width the rate of latent heat release per unit rift length is constant. In other words, one can expect the same undercooling and consequently one constant growth velocity v_g of a dendritic solidification front perpendicular to each rift edge. For these conditions, a rift pulled apart with a velocity $v > v_g$ can maintain constant width only if it grows at an angle to the x axis. This characteristic angle can be easily obtained from trigonometry:

$$\varphi = \arccos(v_g/v)\,.$$

Fits of the experimental data by the geometrical model give excellent agreement. As shown in Fig. 5, the experimental data may also support two regimes for low and high spreading rates, suggesting a more complex pattern formation mechanism. In particular, stresses generated by wax shrinkage, which lead to the deformation of the crust, are not included. The fit to the data gave for $120 \le v \le 266$ μm/sec an onset speed of 78.9 μm/sec and for $v > 266$ μm/sec an onset speed of 116.9 μm/sec.

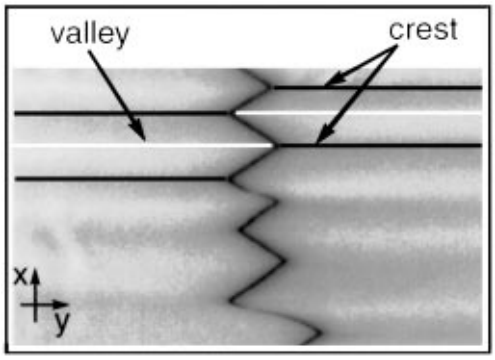

FIG. 4. Zigzag pattern ($v = 241$ μm/sec, $t = 1200$ sec, width = 8.7 cm) showing the three-dimensional structure behind the rift. Liquid wax is black. Crystallized solid wax is alternating between dark and bright (for details see text).

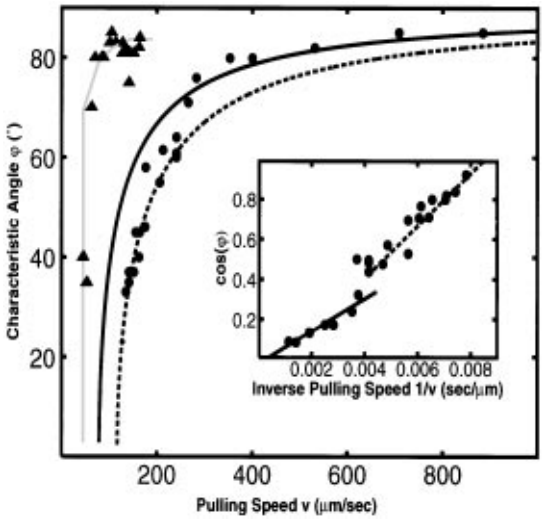

FIG. 5. Characteristic angle vs spreading rate: spiky regime (triangles); zigzag regime (dots). Also shown are the fits by the geometrical model for $120 \le v \le 266$ μm/sec (solid line) and $v > 266$ μm/sec (dashed line). The grey line is a guide to the eye.

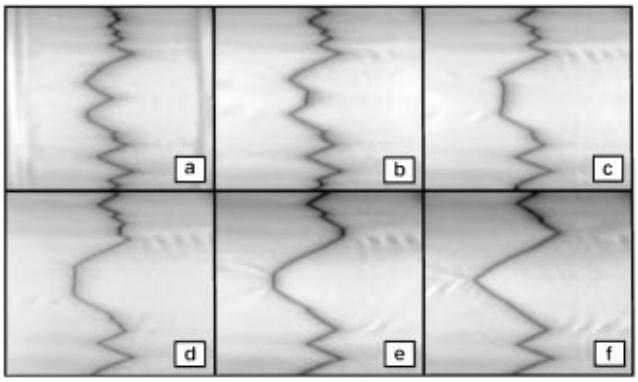

FIG. 6. Coarsening of rift pattern at $v = 213\ \mu$m/sec. The images in the sequence are taken 210 sec apart and each has a width of 20 cm.

So far only static properties of the rift formation have been discussed. Because of the complexity of the pattern evolution in spiky regime we limit our discussion to the zigzag regime. As shown in Fig. 6 a well-developed zigzag pattern coarsened by decreasing the number apices in steps of two. The coarsening process was always initiated at an apex of the rift pattern, where the apex developed into a straight front parallel to the x axis which propagated with a velocity equal to or less than $\frac{1}{4}$ of the spreading rate. It moved under constant deceleration so as to create a new apex on the opposite side and to eliminate the two adjacent apices. Sometimes we observed multiple coarsening processes (as visible in Fig. 6), but due to the finite length of the experiment we could not capture the late stages of the coarsening process. The coarsening itself is only explainable by an asymmetrical growth process that allows the rift edge on one side to grow faster than the opposite one. This behavior is totally unaccounted for in the geometrical model, and we believe that the nonlocal stress field due to the shrinkage of the wax is an important factor in the coarsening process. In particular, the wavy topology behind the apices in Fig. 6 may be contributed to stresses in the crust.

In conclusion, we have shown that the rift pattern phase diagram is surprisingly complex. For the zigzag regime the geometrical model leads directly to the steep angles needed for the development of faultlike structures. Although the wax experiment may not model the physical processes relevant for the ocean floors, the system presented above offers the possibility of testing more general nonlinear models for rift formation. From the pattern formation point of view, the geometrical model describing the zigzag pattern should be universal. Indeed, the same model was found to explain triangular disclination lines in an experiment of directional solidification of nematic liquid crystals [11]. In another experiment on magnetic domains in amorphous iron films, similar zigzag patterns were observed [12], and we believe that in this case the zigzag structure may be triggered by a competition of the imposed velocity, given by the switch-on time of the magnetic field and the intrinsic propagation velocity of the domain walls.

E. B. thanks B. Shaw for bringing this problem to his attention. We have benefited from discussions with G. Barkema, M. Grant, J. Guckenheimer, T. Molteno, S. Morris, K. Satyanarayan, D. Turcotte, and S. Watanabe, as well as from the contributions by the technical personnel of the Laboratory for Atomic and Solid State Physics. Shell Development Co. graciously supplied paraffin wax samples. We also thank C. Franck, U. Happek, and A. Sievers for providing equipment in the initial stages of the experiment. This work was supported by the Alfred P. Sloan Foundation and the National Science Foundation under Contract No. DMR-9121654. J. L. F. acknowledges support from the undergraduate program of the Material Science Center at Cornell University.

*Present address: Harvard University, Cambridge, MA 02138.
†Electronic address: eb22@cornell.edu

[1] See, for instance, M. C. Cross and P. C. Hohenberg, Rev. Mod. Phys. **65**, 851 (1993), and references therein.
[2] See, for instance, *Handbook of Crystal Growth*, edited by D. T. J. Hurle (North-Holland, Amsterdam, 1993), and references therein.
[3] See, for instance, A. Yuse and M. Sano, Nature (London) **362**, 329 (1993); O. Ronsin, F. Heslot, and B. Perrin, Phys. Rev. Lett. **75**, 2352 (1995); C. Allain and L. Limat, Phys. Rev. Lett. **74**, 2981 (1995).
[4] D. W. Oldenburg and J. N. Brune, Science **178**, 301 (1972).
[5] D. W. Oldenburg and J. N. Brune, J. Geophys. Res. **80**, 2575 (1975).
[6] J. W. O'Bryan, R. Cohen, and W. N. Gilliard, Geophys. Soc. Am. Bull. **86**, 793 (1975).
[7] M. Kruskal and H. Segur, *Asymptotics Beyond All Orders in a Model of Dendritic Growth* Aero. Res. Assn. of Princeton Tech. Memo (1985); Y. Pomeau and M. Ben Amar, in *Solids Far From Equilibrium*, edited by C. Godrèche (Cambridge University Press, Cambridge, 1992), p. 400.
[8] R. van der Vennet, Shell Development Co., Houston, Texas (private communication).
[9] The physical properties of Shellwax 120 are best captured by the macroscrystalline paraffin wax of melting point 53 °C described in *Paraffin Products*, edited by G. Mózes (Elsevier Scientific Publishing Co., Amsterdam, 1982).
[10] The heat of fusion of Shellwax 120 is $L \approx 200$ J/g [8] and the thermal diffusivity is $\kappa = 3 \times 10^{-9}$ m^2/sec [9].
[11] J. Bechhoefer, thesis, University of Chicago, 1988 (unpublished); P. Oswald, J. Bechhoefer, and A. Libchaber, Phys. Rev. Lett. **58**, 2318 (1987).
[12] H. Boersch and M. Lambeck, Z. Phys. **159**, 248 (1960).